



3 4456 0266730 8

ORNL/TM-10363

oml

OAK RIDGE
NATIONAL
LABORATORY

MARTIN MARIETTA

Feasibility of Alpha Particle Measurement in a Magnetically Confined Plasma by CO₂ Laser Thomson Scattering

R. K. Richards
K. L. Vander Sluis
D. P. Hutchinson

OAK RIDGE NATIONAL LABORATORY
CENTRAL RESEARCH LIBRARY
CIRCULATION SECTION
4000 BOON 101
LIBRARY LOAN COPY
DO NOT TRANSFER TO ANOTHER PERSON
If you wish someone else to see this
report, send its name with report and
the library will arrange a loan.

OPERATED BY
MARTIN MARIETTA ENERGY SYSTEMS, INC.
FOR THE UNITED STATES
DEPARTMENT OF ENERGY

Printed in the United States of America. Available from
National Technical Information Service
U.S. Department of Commerce
5285 Port Royal Road, Springfield, Virginia 22161
NTIS price codes—Printed Copy: A03; Microfiche A01

This report was prepared as an account of work sponsored by an agency of the United States Government. Neither the United States Government nor any agency thereof, nor any of their employees, makes any warranty, express or implied, or assumes any legal liability or responsibility for the accuracy, completeness, or usefulness of any information, apparatus, product, or process disclosed, or represents that its use would not infringe privately owned rights. Reference herein to any specific commercial product, process, or service by trade name, trademark, manufacturer, or otherwise, does not necessarily constitute or imply its endorsement, recommendation, or favoring by the United States Government or any agency thereof. The views and opinions of authors expressed herein do not necessarily state or reflect those of the United States Government or any agency thereof.

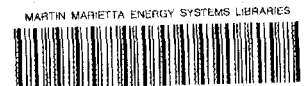
Physics Division

FEASIBILITY OF ALPHA PARTICLE MEASUREMENT
IN A MAGNETICALLY CONFINED PLASMA BY
CO₂ LASER THOMSON SCATTERING

R. K. Richards, K. L. Vander Sluis, and D. P. Hutchinson

Date Published - August 1987

Prepared by the
OAK RIDGE NATIONAL LABORATORY
Oak Ridge, Tennessee 37831
operated by
MARTIN MARIETTA ENERGY SYSTEMS, INC.
for the
OFFICE OF FUSION ENERGY
U.S. DEPARTMENT OF ENERGY
under Contract No. DE-AC05-84OR21400



3 4456 0266730 8

CONTENTS

	<u>Page</u>
Abstract	1
Introduction	1
Scattering Geometry	2
Rectangle of Detection	11
Optimizing Detection	14
Signal to Noise	16
Conclusions	21
References	22

FEASIBILITY OF FUSION-PRODUCT ALPHA PARTICLE MEASUREMENT
IN A MAGNETICALLY CONFINED PLASMA BY
CO₂ LASER THOMSON SCATTERING

R. K. Richards, K. L. Vander Sluis, and D. P. Hutchinson

ABSTRACT

Fusion-product alpha particles will dominate the behavior of the next generation of ignited D-T fusion reactors. Advanced diagnostics will be required to characterize the energy deposition of these fast alpha particles in the magnetically confined plasma. For small-angle coherent Thomson scattering of a CO₂ laser beam from such a plasma, a resonance in the scattered power occurs near 90° with respect to the magnetic field direction. This spatial concentration permits a simplified detection of the scattered laser power from the plasma using a heterodyne system. The signal produced by the presence of fusion-product alpha particles in an ignited plasma is calculated to be well above the noise level, which results from statistical variations of the background signal produced by scattering from free electrons.

INTRODUCTION

In previous studies of alpha particle Thomson scattering the emphasis was on either experimental requirements in the absence of a magnetic field¹ or on the theory describing the resonance produced in the presence of a magnetic field.² The purpose of this report is to combine the aspects of the theory which includes magnetic-field effects with the experimental requirements for detection of the scattered signal produced by the alpha particles. Using the extended theory, the signal to noise calculations for heterodyne detection are re-evaluated and an estimate

made of the detection limit for determining the presence of high-energy alpha particles in a plasma.

SCATTERING GEOMETRY

The scattering geometry is shown schematically in Fig. 1. This figure depicts the three important scattering angles: θ_0 , $\Delta\theta$, and ϕ . Here θ_0 defines the forward scattering angle between the centroids of the CO₂ laser beam and the detector antenna pattern, $\Delta\theta$ is the divergence angle for the detector antenna pattern, and ϕ is the angle of scattered signal with respect to the magnetic field direction. The divergence angle for the detector antenna pattern, $\Delta\theta$, is an important parameter in determining the scattered signal power on the detector. This angle defines the solid angle over which the detector collects signal (an integration in both θ and ϕ) and is related to the scattering volume in the plasma over which the detector will receive signal (i.e., the intersection of the antenna pattern and the CO₂ laser beam). The antenna pattern can be created by a second laser which operates near the CO₂ laser frequency. This second laser is generally referred to as a local oscillator. Figure 2 shows the laser beam envelope, and illustrates the relation between the divergence angle, $\Delta\theta$, and the radius, W , of the local oscillator. The minimum radius, W_0 , referred to as the waist, determines the radius along the path of the local oscillator by³

$$W/W_0 = 1 + \left(\frac{Z\lambda}{\pi W_0^2}\right)^2, \quad (1)$$

where Z is the distance along the laser path from the waist position and λ is the wavelength. For $W \gg W_0$

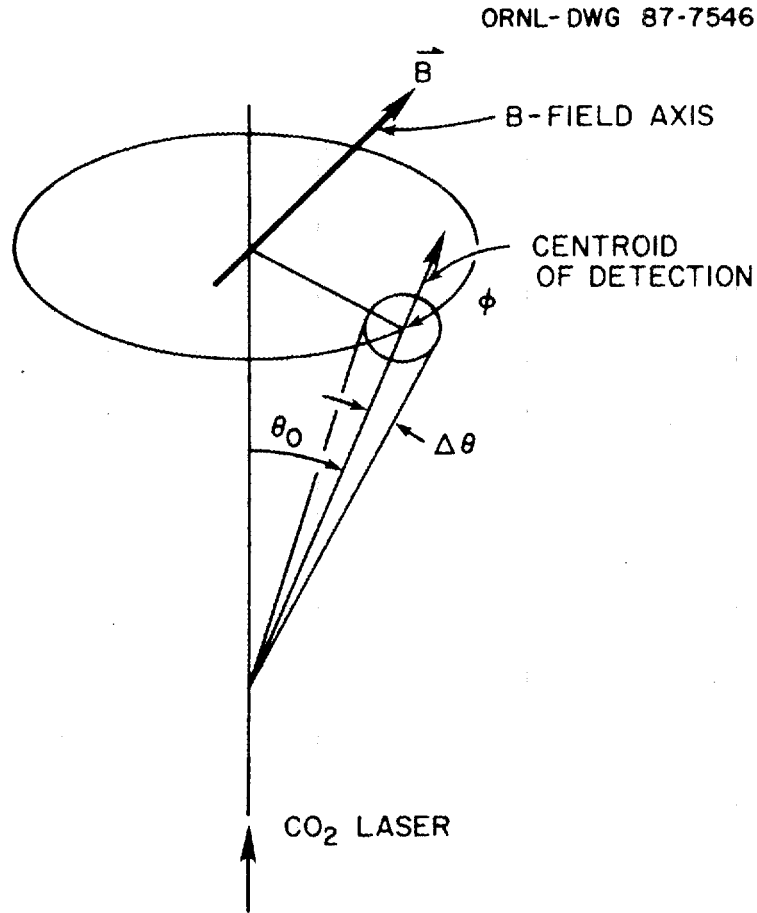


Fig. 1. Laser scattering geometry showing the relation of θ , $\Delta\theta$, and ϕ .

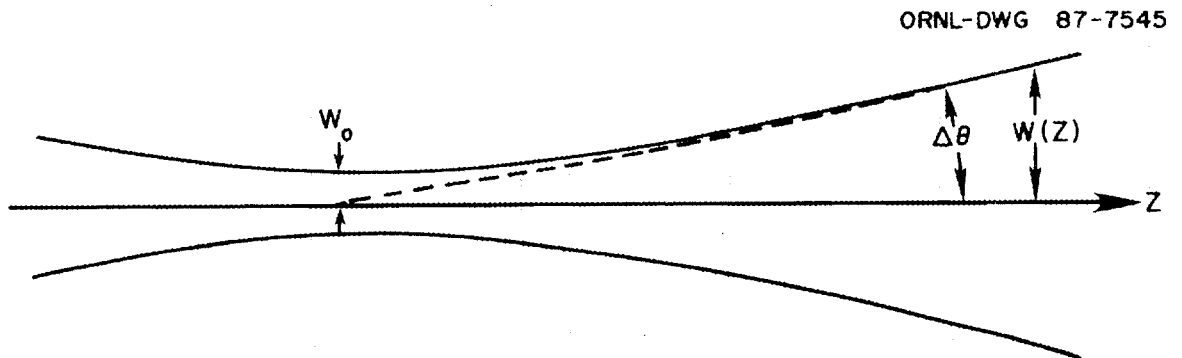


Fig. 2. Shape of the laser beam as it passes through a focus of radius W_0 (the waist). The divergence of the beam, $\Delta\theta$, is related to the waist in Eq. (2).

$$\Delta\theta \cong \frac{\lambda}{\pi W_0} \quad \text{or} \quad W_0 \cong \frac{\lambda}{\pi\Delta\theta} , \quad (2)$$

which relates the divergence to the size of the waist. To maximize the detected signal, the beam from the local oscillator will have the same waist as the CO₂ laser beam and the intersection will occur at the waist position. The frequency of the local oscillator will be shifted from the CO₂ laser line at 28,306 GHz ($\lambda = 10.6 \mu\text{m}$) by less than 20 GHz for alpha particle detection, therefore the wavelength of this beam will also be approximately 10.6 μm .

The length, L, of intersection between the CO₂ laser beam and the local oscillator is an important factor in determining the scattered signal collected by the detector. For a small scattering angle, θ_0 , and a smaller divergence angle $\Delta\theta$ then⁴

$$L \approx \frac{2W_0}{\sin\theta_0} \quad (3)$$

or from Eq. (2)

$$L \approx \frac{2\lambda}{\pi\Delta\theta\sin\theta_0} . \quad (4)$$

Therefore, the selection of the scattering angle and solid angle collecting optics for the detector will determine the length in the plasma along the laser path over which the signal originates.

SPECTRAL DENSITY FUNCTION

The power, P_s , scattered into the solid angle $d\Omega$ over a frequency interval $d\omega$ is given by⁵

$$P_s(\vec{R}, \omega) d\Omega d\omega = P_1 r_0^2 n_e L S(\vec{k}, \omega) d\Omega \frac{d\omega}{2\pi} \quad (5)$$

where P_1 is the incident laser power, r_0 is the classical electron radius, n_e is the electron density, L is the detected scattering length, and $S(\vec{k}, \omega)$ is the spectral density function. The spectral density function can be divided into individual contributions from each species with plasma. For the presence of electrons, primary plasma ions, and alpha particles:

$$S(\vec{k}, \omega) = S_e(\vec{k}, \omega) + S_i(\vec{k}, \omega) + S_\alpha(\vec{k}, \omega) \quad (6)$$

To simplify the calculations for this report it is assumed that all frequency shifts are sufficiently large ($f > 5$ GHz) such that contributions from the primary plasma ion can be ignored.² It is also assumed that $\omega \ll \Omega_e$ and $\Omega_e/k_{\parallel}a \gg 1$, these select the scattering frequency and angle for the region where alpha particle scattering occurs, thus permitting a simplified representation of the spectral density function:

$$S_e(\vec{k}, \omega) \approx \frac{1}{|\epsilon_L|^2} \frac{2\pi^{1/2}}{k_{\parallel}a} e^{-k_{\perp}^2 \rho_e^2} I_0(k_{\perp}^2 \rho_e^2) e^{-\left(\frac{\omega}{k_{\parallel}a}\right)^2} \quad (7)$$

$$S_i(\vec{k}, \omega) \approx 0 \quad (8)$$

$$S_\alpha(\vec{k}, \omega) \approx \frac{|\alpha^2 [R_\omega(\zeta_e) - iI_\omega(\zeta_e)]^2}{|\epsilon_L|^2} 4 \frac{n_\alpha}{n_e} \frac{2\pi}{|k|} f_\alpha^1(\omega/k) \quad (9)$$

where

$$\epsilon_L \approx 1 + H_e \quad (10)$$

$$H_e \approx \alpha^2 \left\{ 1 + e^{-k_{\perp}^2 \rho_e^2} I_0(k_{\perp}^2 \rho_e^2) \left[R_\omega\left(\frac{\omega}{k_{\parallel}a}\right) - iI_\omega\left(\frac{\omega}{k_{\parallel}a}\right) - 1 \right] \right\} \quad (11)$$

and

$$\begin{aligned}
 \zeta_e &= \frac{\alpha}{\sqrt{2}} \frac{\omega}{W_{pe}} \\
 \alpha &= (k \lambda d_e)^{-1} \\
 k_{\parallel} &= k \cos \phi \\
 k_{\perp} &= k \sin \phi \\
 k &= \frac{2\pi}{\lambda} 2 \sin (\theta/2)
 \end{aligned} \tag{12}$$

Here ρ_e is the electron gyroradius, Ω_e the electron cyclotron frequency, W_{pe} the electron plasma frequency, and $a = (2 kT_e/m_e)^{1/2}$ the mean thermal electron velocity. The functions $R_{\omega}(\chi)$ and $I_{\omega}(\chi)$ are derived from the plasma dispersion function $Z(\chi)$ according to

$$1 + \chi Z(\chi) = R_{\omega}(\chi) - i I_{\omega}(\chi) \tag{13}$$

which is available in tabulated form.⁶ The function $f_{\alpha}^1(\omega/k)$ is the one-dimensional velocity distribution of the alpha particles and is determined by the form of the distribution function. For all calculations in this report the alpha particles are assumed to have the standard slowing-down distribution⁷ where

$$f_{\alpha} = \begin{cases} \frac{F_0}{v^3 + v_c^3}, & v < v_{\alpha} \\ 0, & v > v_{\alpha} \end{cases} \tag{14}$$

which was also used in Ref. 2. For this distribution

$$f_{\alpha}^1(u) = \frac{-2\pi F_0}{3v_c} \left[\frac{1}{2} \ln \left\{ \frac{(y + v_c)^2}{y^2 - yv_c + v_c^2} \right\} - \sqrt{3} \tan^{-1} \left(\frac{2y - v_c}{\sqrt{3} v_c} \right) \right]_{y = |u|}^{y = v_{\alpha}} \tag{15}$$

and F_0 is determined by the normalization

$$\int_{-\infty}^{+\infty} f_{\alpha} d^3v = 1 \tag{16}$$

The influence of the magnetic field enters into the scattering through the size of the electron gyro orbit and the angle ϕ .

The expected plasma conditions and the CO₂ laser specifications necessary for measuring the alpha-particle scattering for the specific case of the TFTR device are given in Table 1; these are the same conditions which were applied in previous investigations.^{1,2} Under these

Table I. Plasma and laser parameters

$n_e = 1.2 \times 10^{14} \text{ cm}^{-3}$	$T_e = 10 \text{ keV}$
$n_i = 1.185 \times 10^{14}$	$T_i = 10 \text{ keV}$
$n_\alpha = 7.5 \times 10^{11}$	$E_\alpha < 3.5 \text{ MeV}$
$P_i = 100 \text{ MW}$	$\lambda_i = 10.6 \text{ } \mu\text{m}$
$B_0 = 5 \text{ T}$	$\tau_{\text{laser}} = 1 \text{ } \mu\text{s}$

conditions the scattering was predicted to exhibit a resonance.² This resonance is produced by a cancellation of the terms contributing to the dielectronic function, ϵ_L , causing it to become quite small for particular values of θ , ϕ , or frequency f . Because the dielectric function enters into both the free-electron and alpha-particle scattering [see Eqs. (7) and (9)] both will exhibit the same resonance. This is illustrated in Fig. 3, which shows the variation of the spectral density functions with the angle ϕ . A clear resonance appears near $\phi = 85^\circ$ (and from symmetry, $\phi = 95^\circ$) for both species. The angular position of the resonance is dependent on the values of n_e , T_e , B , f , and θ . For the values of n_e , T_e , and B listed in Table 1 the resonance will exist near

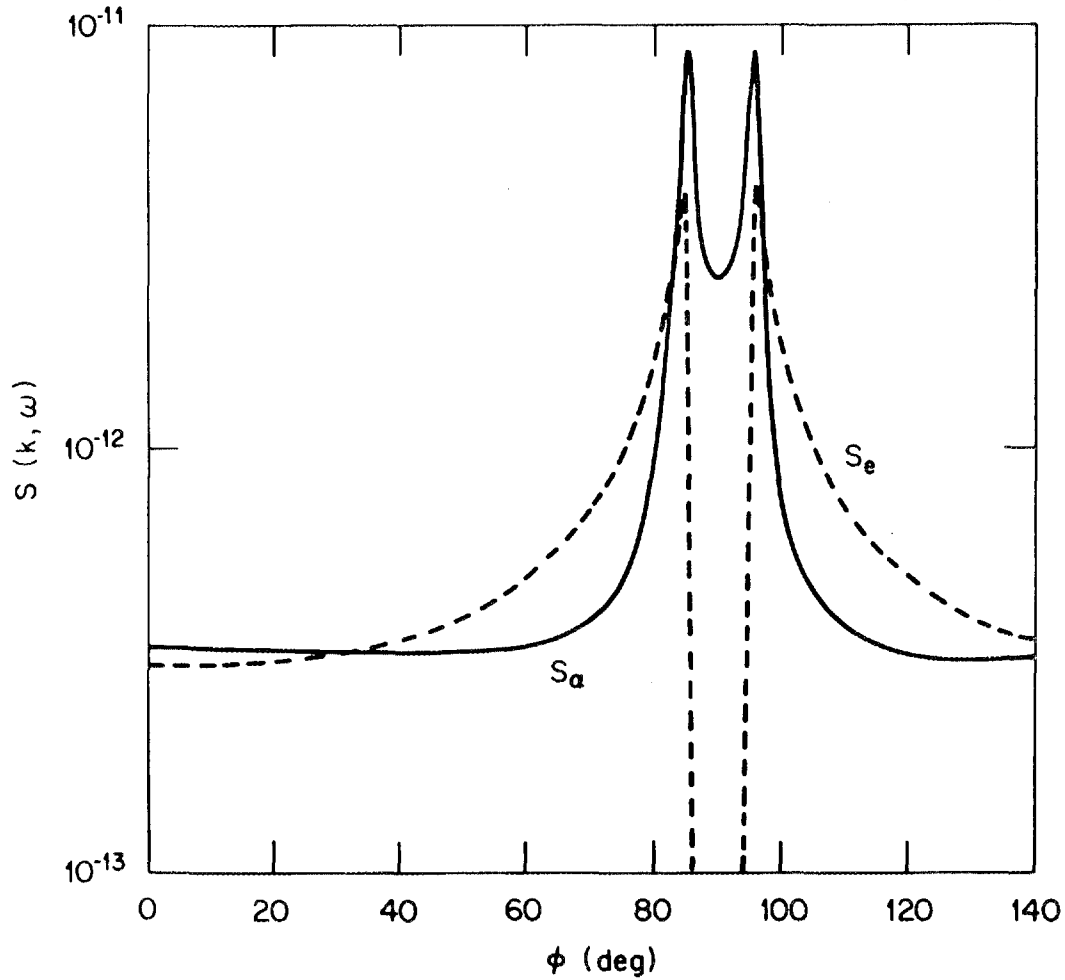


Fig. 3. The spectral density function versus ϕ , the angle with respect to the magnetic field direction. The frequency shift is 11 GHz and the scattering angle, θ , is 0.7 degrees.

$\phi = 90^\circ$ for all f , the frequency shift, and θ of interest for alpha-particle detection (i.e., $5 \text{ GHz} < f < 20 \text{ GHz}$, $0.5^\circ < \theta < 1^\circ$). For smaller frequency shifts the resonance moves closer to 90° as shown in Fig. 4 and at smaller scattering angles the amplitude of the scattering increases as shown in Fig. 5.

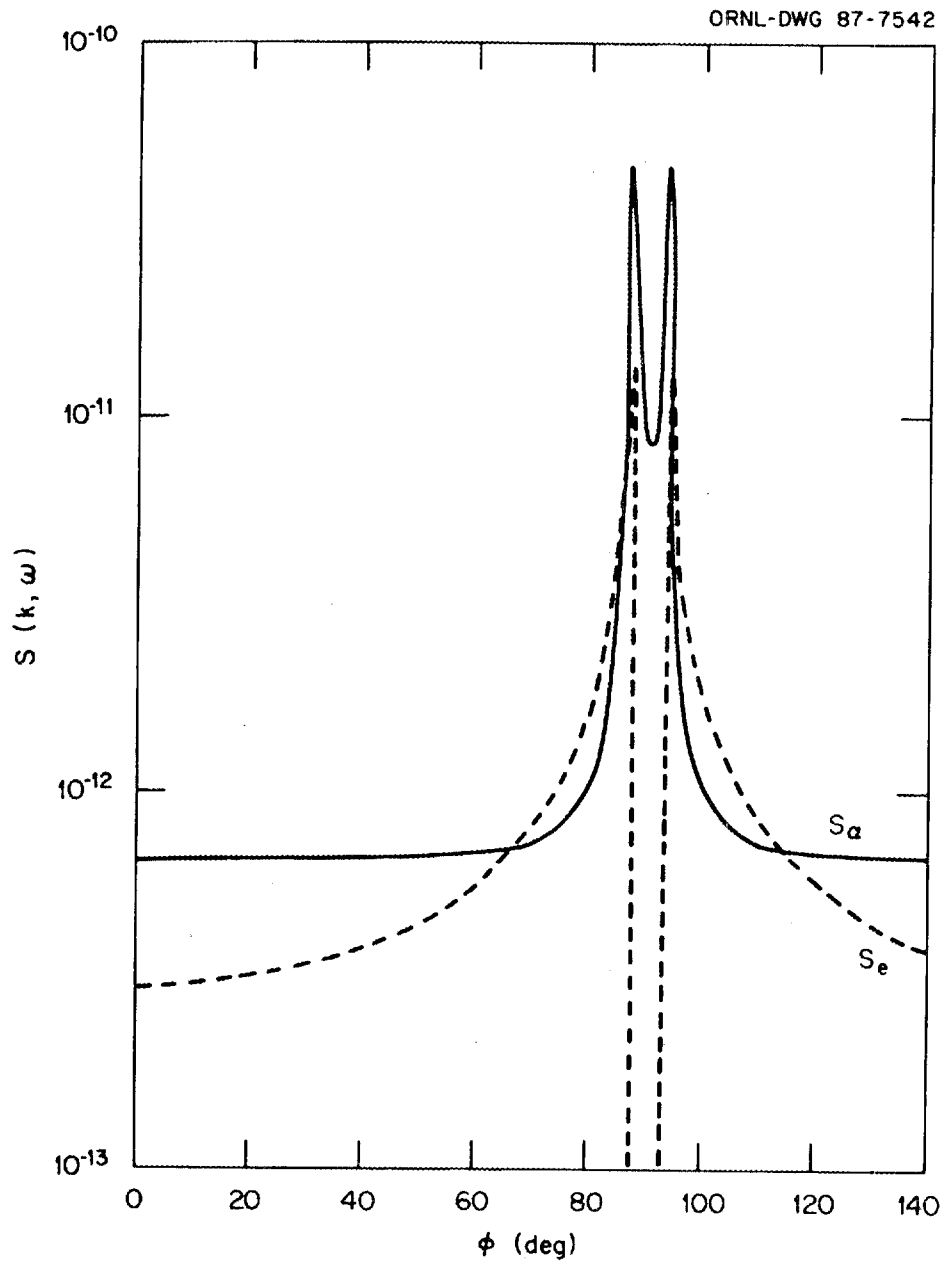


Fig. 4. The spectral density function versus ϕ , the angle with respect to the magnetic field direction. The frequency shift is 7 GHz and the scattering angle, θ , is 0.7 degrees.

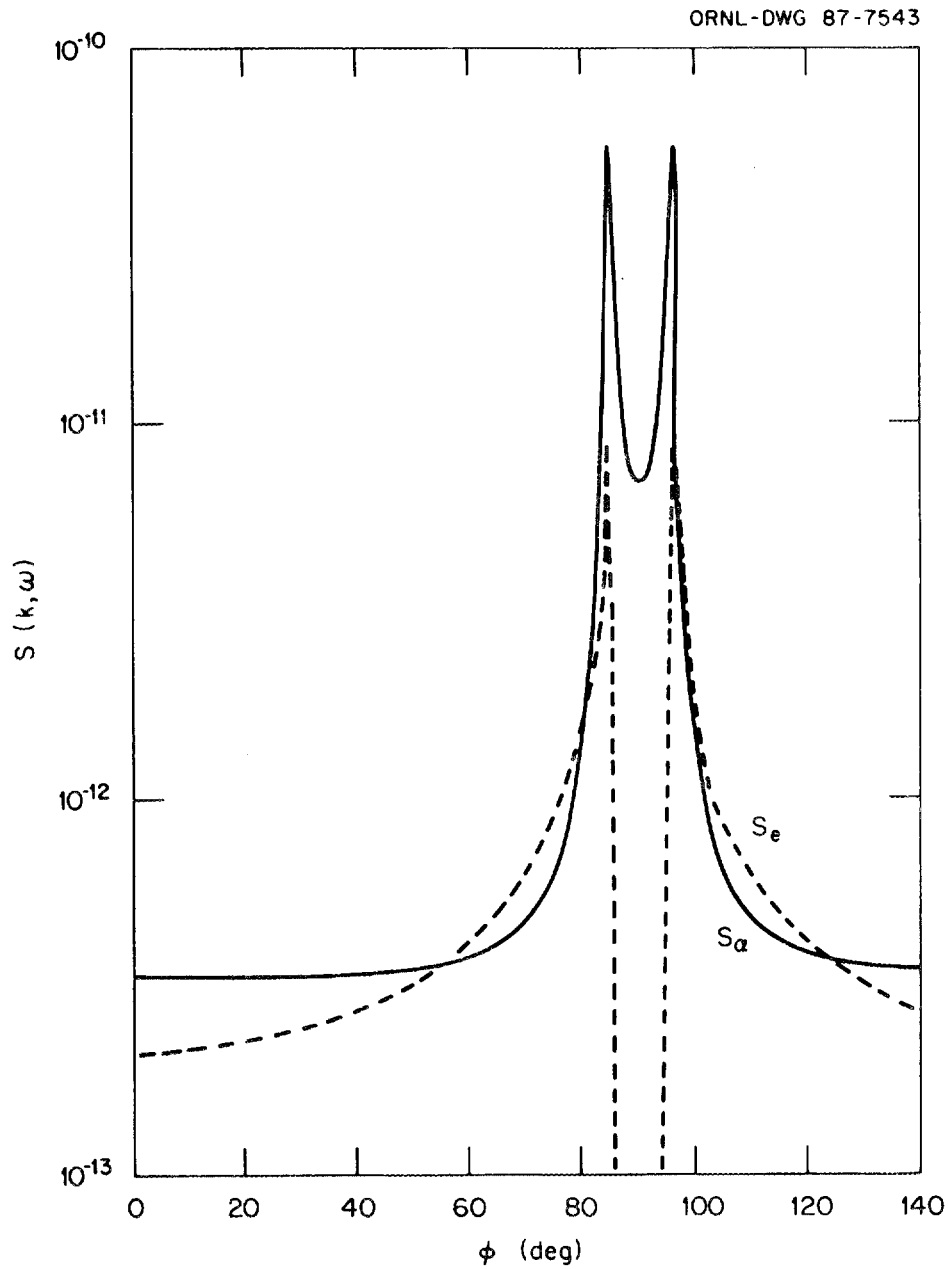


Fig. 5. The spectral density function versus ϕ , the angle with respect to the magnetic field direction. The frequency shift is 11 GHz and the scattering angle, θ , is 0.6 degrees.

Because of the spatial variation of the scattering intensity, by detecting the scattered signal near $\phi = 90^\circ$ with only a small solid angle, it is possible to collect nearly half of the total scattered power; the other half can be collected around $\phi = 270^\circ$. By reducing the solid angle of detection it may also be possible to substantially reduce the electron scattered signal since this is zero at $\phi = 90^\circ$ where the alpha-particle signal is still large.

Before discussion of the signal optimization with appropriate angular selection it is necessary to consider alpha particle energy selection.

RECTANGLE OF DETECTION

The Thomson scattering of the CO₂ laser due to the presence of the alpha particles in the plasma is a matching of the phase velocity of the scattered photons with the component of the alpha particle velocity in the direction of scattering; i.e.,

$$\omega/k = v_{\parallel} . \quad (17)$$

Using the relation between the wave number k and the scattering angle θ and noting that $v_{\parallel} < v$ then Eq. (17) gives the inequality

$$f(\text{GHz})/\theta(\text{deg}) < 11.5 \sqrt{\epsilon(\text{MeV})} . \quad (18)$$

As noted earlier in the comparison of Figs. 3 and 5, the scattered power is sensitive to small changes in the scattering angle θ , with much greater scattering intensity occurring at the smaller angles. This is equivalent to having the inequality 18 becoming an equality;

$$f(\text{GHz})/\theta(\text{deg}) \approx 11.5 \sqrt{\epsilon(\text{MeV})} . \quad (19)$$

Therefore, a particular selection of frequency and scattering angle will uniquely define the energy of the alpha particles being detected. In an experiment, each detection channel will have a range of frequencies and scattering angles which leads to a range in energy over which it is sensitive. Each detection channel can be represented by a rectangle in the f - θ plane with straight lines representing contours of constant energy, the corners of this rectangle will represent the extremes in energy. An example of this is given in Fig. 6. Here two detectors are depicted each with a bandwidth of 3 GHz and an angular detection between 0.5° and 0.75° with one centered at 11 GHz and the other centered at 7 GHz. From the corners in the rectangle of detection the 7 GHz detector is found to be sensitive to alpha particles between 0.41 and 2.19 MeV and the 11 GHz detector between 1.21 and 4.73 MeV. Since alpha particles are created with 3.5 MeV of kinetic energy there will be few with energies above this and the 11 GHz detector will be clipped along the 3.5 MeV line.

As illustrated in Fig. 6, for a fixed scattering angle θ , the large alpha particle energies scatter at the larger frequencies. For frequencies above 11 GHz the scattering will occur only into angles greater than 0.5° . However, the scattered power for the alpha particles decreases rapidly with increasing scattering angle. Using 0.5° as an absolute practical minimum for the scattering angle, the higher energy particles in the alpha particle distribution can be readily detected at a frequency shift of 11 GHz, lower frequency shifts will be more sensitive to lower energies and higher frequency shifts will suffer a greatly decreased signal.

ORNL-DWG 87-7544

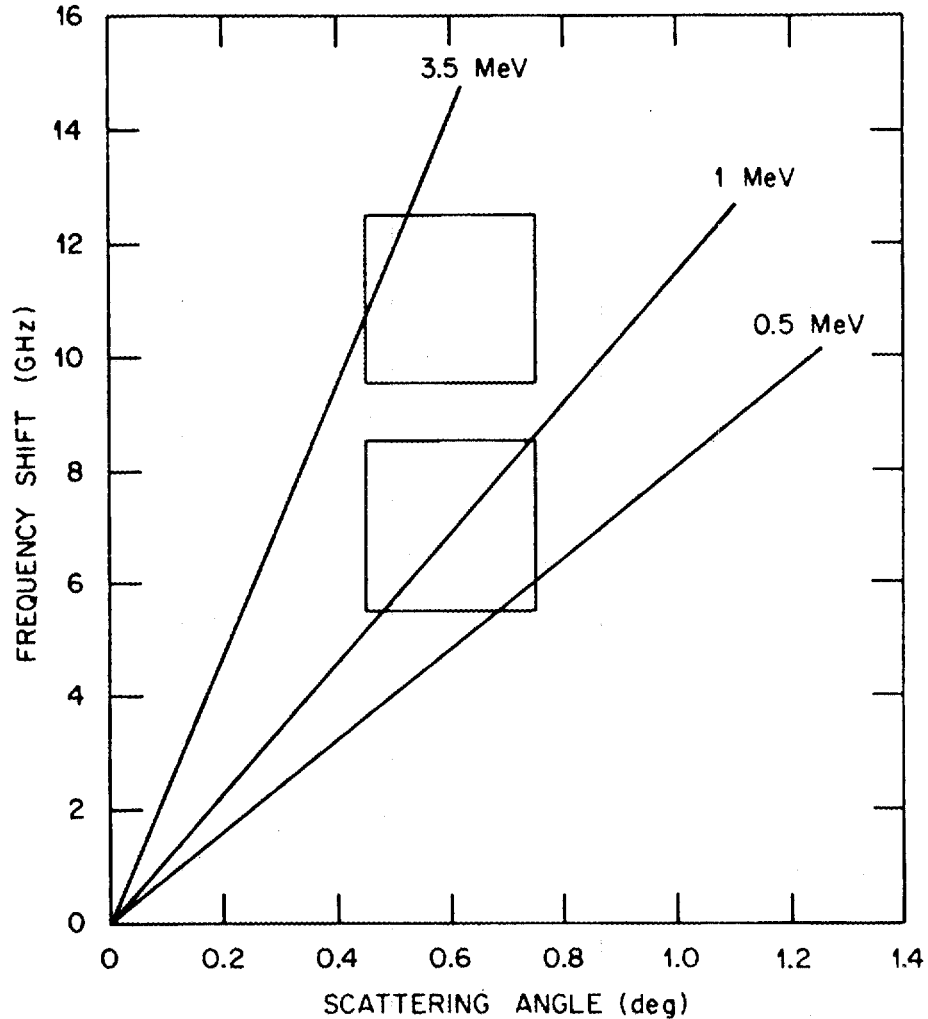


Fig. 6. The rectangle of detection — showing contours of constant alpha particle energy in the f - θ plane. The range of this energy for each detector is determined by the rectangle formed by the limit of f (frequency bandwidth) and range of scattering angles. The two detectors represented are centered at 7 GHz and 11 GHz from the CO_2 laser frequency and each has a 3 GHz bandwidth and an angular extent between 0.5 and 0.75 degrees.

For a detector centered at the 7 GHz frequency shift, the intermediate energy particles will be sampled. These particles will be important in fusion reactors because their presence represents an important heating of the plasma by collisional cooling of alpha particles.

OPTIMIZING DETECTION

Upon selection of a central frequency for a detector, the scattered power into a particular solid angle can be calculated from the derivations in the previous sections. For example, with selection of the 7 GHz shift from the CO₂ laser line, which is sensitive to the intermediate energy alpha particles, a plot of the scattered power for both alpha particles and free electrons versus the angular divergence of the detector antenna pattern is given in Fig. 7. For this calculation it was assumed that the minimum scattering angle being detected remained fixed at 0.5°. Figure 7 shows the interesting result that there is an optimal detector antenna pattern for the scattered alpha particle signal. This occurs because most of the scattered power is into a very small solid angle. By increasing the collection solid angle beyond this minimum, very little increase in signal results. However, increasing the solid angle for signal collection decreases the length in the plasma over which signal is detected according to Eq. (4). The balance between maximizing the length and the collection solid angle produces the shape of the scattered power from alpha particles given in Fig. 7. The electron signal does not exhibit this behavior because the electron signal increases rapidly for the larger scattering angles.

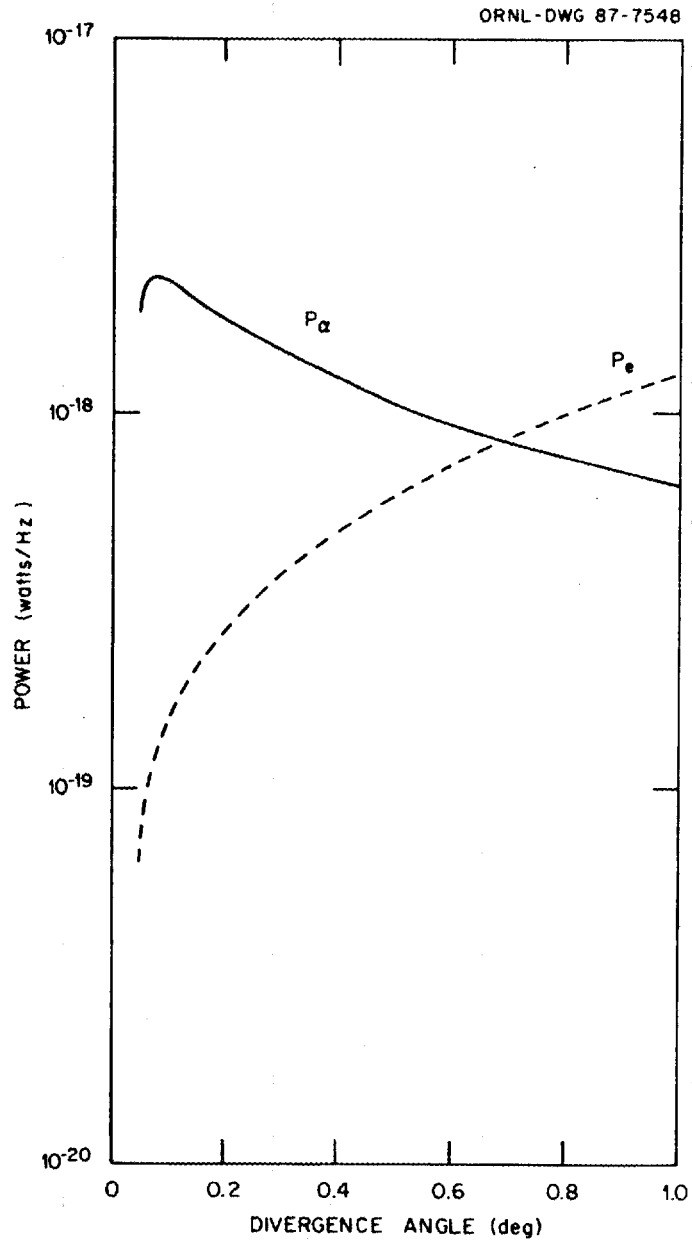


Fig. 7. The scattered power versus the divergence angle, $\Delta\theta$, for both the alpha particles (solid curve) and the free electrons (dashed curve). The frequency shift is 7 GHz and the minimum scattering angle, θ , is fixed at 0.5 degrees.

Other frequencies will exhibit a similar behavior. For a detector channel shifted 11 GHz from the CO₂ laser line, the scattered power versus detector divergence angle is given in Fig. 8. For this frequency the scattered power from the alpha particles is slightly smaller and has a peak at a larger $\Delta\theta$ than that for a detector channel at 7 GHz. Note that the electron scattered power is also slightly smaller. A plot of the frequency dependence for $\Delta\theta = 0.125^\circ$ is given in Fig. 9. The sharp reduction in signal for frequencies above 11 GHz is due to the clipping of the rectangle of detection as noted in the previous section. For larger solid angles this effect is not as pronounced, as shown in Fig. 10 for $\Delta\theta = 0.25^\circ$.

SIGNAL TO NOISE

For heterodyne detection the signal to noise ratio has the form¹

$$(S/N)_{PD} = \frac{(S/N)_1}{(S/N)_1 + 1} \sqrt{\Delta f \tau + 1} \quad , \quad (20)$$

where Δf is the detector bandwidth, τ is the laser pulse length, $(S/N)_1$ is the initial signal to noise ratio, and $(S/N)_{PD}$ is the post detection signal to noise ratio. For example, consider a detector shifted 7 GHz from the CO₂ laser line with a 3 GHz bandwidth and optics selected for $\Delta\theta = 0.125^\circ$. Then from Fig. 9, with a detection noise level of 1×10^{-19} W/Hz

$$(S/N)_1 \text{ (alpha)} = 21$$

$$(S/N)_1 \text{ (electron)} = 1.8 \quad (21)$$

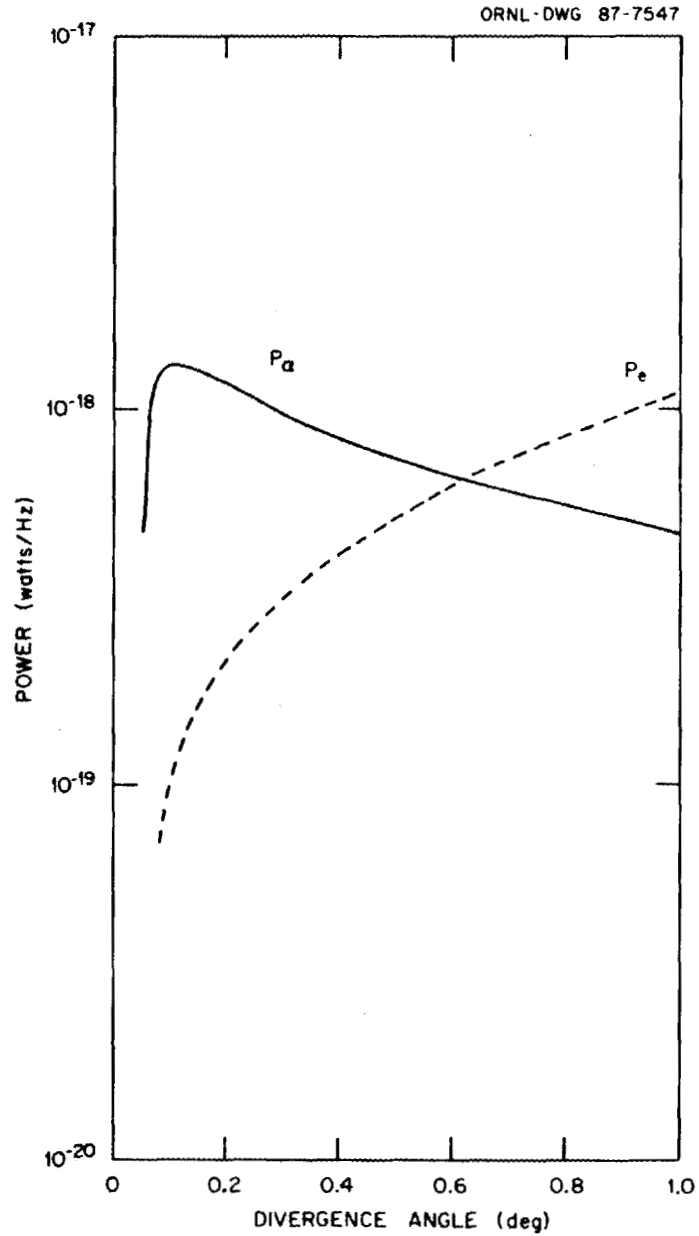


Fig. 8. The scattered power versus the divergence angle, $\Delta\theta$, for both the alpha particles (solid curve) and the free electrons (dashed curve). The frequency shift is 11 GHz and the minimum scattering angle, θ , is fixed at 0.5 degrees.

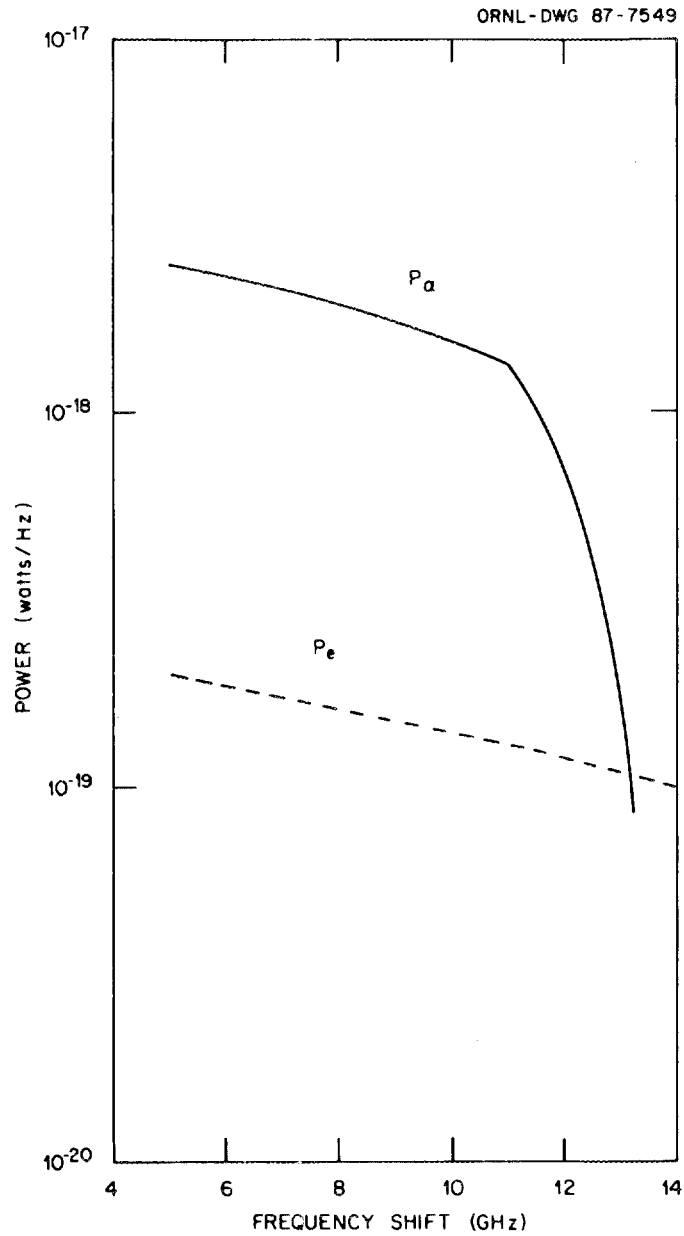


Fig. 9. The frequency dependence of the scattered power for a divergence angle of 0.125° . The solid curve is the scattered power due to the alpha particles and the dashed curve from the free electrons.

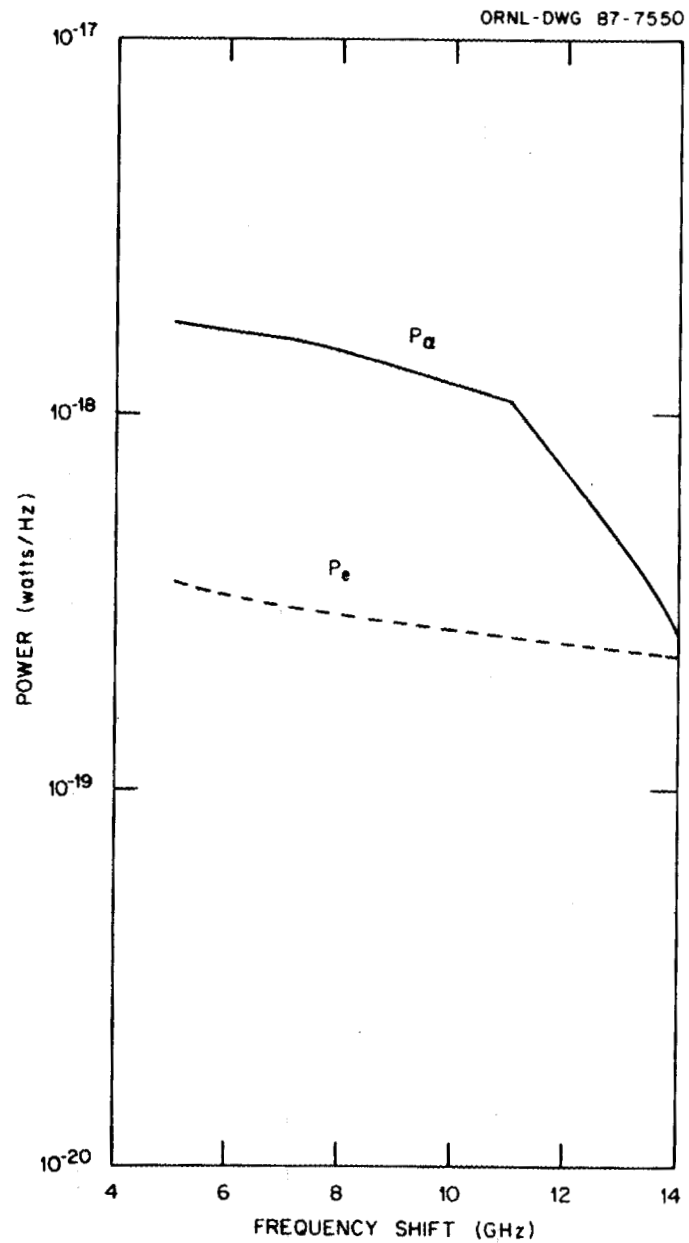


Fig. 10. The frequency dependence of the scattered power for a divergence angle of 0.25° . The solid curve is the scattered power due to the alpha particles and the dashed curve from the free electrons.

For alpha particle detection, the electrons signal will contribute to the noise such that

$$(S/N)_{PD} (\text{alpha}) = \frac{21}{21 + 1.8 + 1} \sqrt{\Delta f \tau + 1} . \quad (22)$$

For a laser pulse length of 1 μ sec the output signal to noise for the alpha particles will be

$$(S/N)_{PD} (\text{alpha}) = 48.3 . \quad (23)$$

Note that any increase in the initial signal to noise will have little effect on the final signal to noise since it is approaching the maximum value of $\sqrt{\Delta f \tau + 1} = 54.8$. To further increase the signal to noise either or both Δf and τ must be increased, but increasing Δf reduces energy resolution, and increasing τ generally reduces input laser power which reduces scattered power.

The detection limit for alpha particles will be set by the background signal from the free electrons in the plasma. With no alpha particles present the signal to noise ratio will be 35.2 from the electrons alone. The variation of $(S/N)_{PD} (\text{alpha})$ with alpha particle density is given in Fig. 11. Note that the alpha particle and electron signals are equal for $N_{\alpha} = 1 \times 10^{11} \text{ cm}^{-3}$. For alpha particle densities above 10^{11} cm^{-3} an accurate estimate of this density can be made from the detected scattered signal with only a slight correction needed for the electron background. If the alpha particle density were in the range 10^{10} to 10^{11} cm^{-3} it would be possible to detect the presence of alphas but the large correction for the electron background would make an accurate density estimate impossible. If the alpha particle density were below 10^{10}

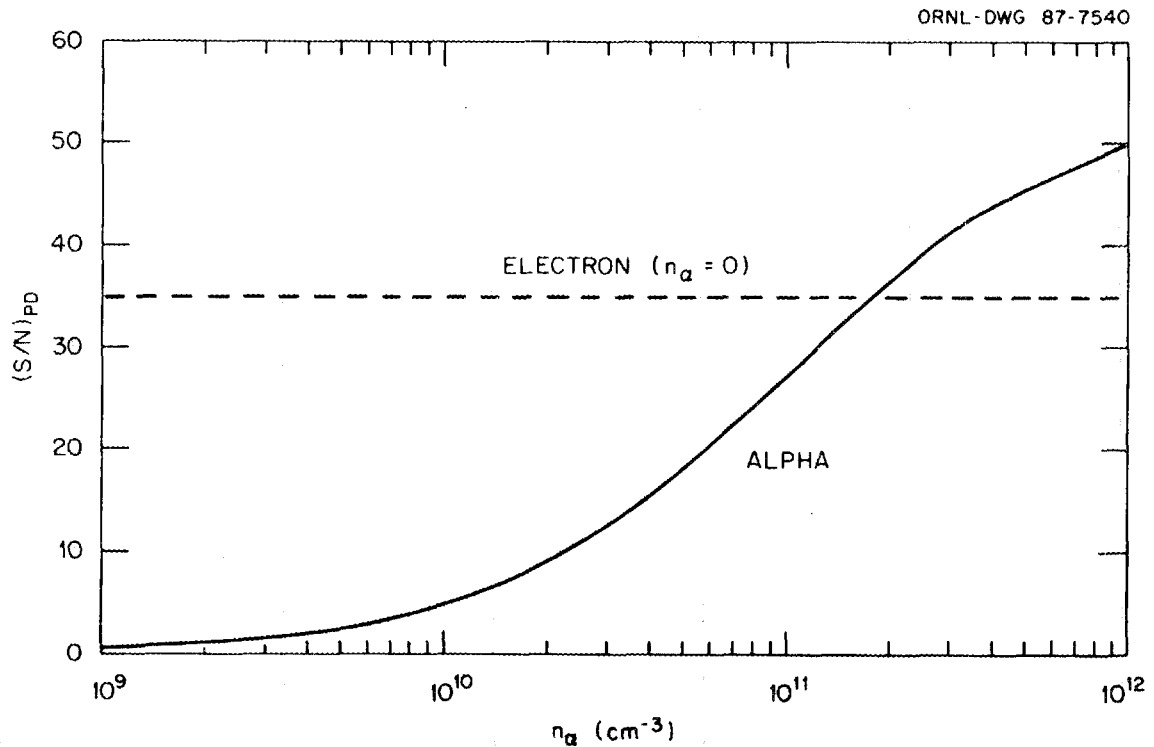


Fig. 11. The post detection heterodyne signal to noise ratio versus alpha particle density. The curves are for electrons alone and the alpha particles with an electron background. The receiver is set at a 7 GHz shift, 3 GHz bandwidth, a 1 μsec pulse length, and a divergence angle of 0.125° .

cm^{-3} even the presence of alphas could not be determined due to the noise generated by the electron signal.

CONCLUSIONS

The effect of the magnetic field on CO_2 Thomson scattering from a magnetically confined burning fusion plasma is primarily a spatial concentration of the scattered alpha particle signal. This permits collection of most of the scattered signal within a small solid angle. Apart from an important improvement in the signal-to-noise ratio, such a

feature has a significant practical advantage in a fusion device which generally has very limited port access available for diagnostics.

The limits for detecting the presence of alpha particles ($n_\alpha = 10^{10} \text{ cm}^{-3}$) or the measurement of the alpha particle density ($n_\alpha = 10^{11} \text{ cm}^{-3}$) are set by the background scattered signal from the thermal plasma electrons. These are well below the expected alpha particle density of $7.5 \times 10^{11} \text{ cm}^{-3}$ expected in TFTR. Therefore it should be feasible to detect variations in the alpha particle density for varying plasma conditions.

For the next generation of fusion experiments, such as the proposed compact ignition torus (CIT), plasma parameters are expected to be somewhat different from those in TFTR; therefore, the alpha particle Thomson scattering will also change. With a higher electron density expected in CIT the alpha particle scattering intensity will be larger and the electron scattering smaller. It then may be possible to use a lower power CO_2 laser which has a sufficient repetition rate to measure the time dependence of the alpha particle density, or to use larger scattering angles in order to perform spatial measurements.

REFERENCES

1. D. P. Hutchinson, K. L. Vander Sluis, J. Sheffield, and D. J. Sigmar, Feasibility of Alpha Particle Measurement by CO_2 Laser Thomson Scattering, ORNL/TM-9090, Martin Marietta Energy Systems, Inc., Oak Ridge Natl. Lab., December 1984.
2. L. Vahala, G. Vahala, and D. J. Sigmar, Nucl. Fusion 25, 51 (1986).

3. A. E. Siegman, Section 8.2 in An Introduction to Lasers and Masers, McGraw-Hill, New York (1971).
4. E. Holzhauser and J. H. Massig, *Plasma Phys.* 20, 867 (1978).
5. J. Sheffield, Plasma Scattering of Electromagnetic Radiation, Academic Press, New York (1975).
6. B. D. Fried and S. D. Conte, The Plasma Dispersion Function, Academic Press, New York (1961).
7. J. D. Gaffey, Jr., *J. Plasma Phys.* 16, 149 (1976).

INTERNAL DISTRIBUTION

- | | |
|-----------------------|------------------------------------|
| 1. J. B. Ball | 17-21. K. L. Vander Sluis |
| 2. W. H. Casson | 22. Fusion Energy Division Library |
| 3. H. T. Hunter | 23. Central Research Library |
| 4-8. D. P. Hutchinson | 24. Document Reference Section |
| 9. C. H. Ma | 25-26. Laboratory Records |
| 10. R. A. Phaneuf | 27. Laboratory Records, RC |
| 11-15. R. K. Richards | 28. ORNL Patent Section |
| 16. J. Sheffield | |

EXTERNAL DISTRIBUTION

29. Office of the Assistant Manager for Energy Research and Development, Department of Energy, Oak Ridge Operations, Box E, Oak Ridge, TN 37831
30. C. A. Bennett, Dept. of Physics, Univ. of North Carolina-Asheville, Asheville, NC 28814
31. Bibliothek, Institut fur Plasmaphysik, KFA, Postfach 1913, D-5170 Julich, Federal Republic of Germany
32. Bibliothek, Max-Planck Institut fur Plasmaphysik, D-8046 Garching bei Munchen, Federal Republic of Germany
33. Bibliotheque, Centre de Recherches en Physique des Plasmas, 21 Avenue des Bains, 1007 Lausanne, Switzerland
34. Bibliotheque, Service due Confinement des Plasma, CEA, B.P. 6, 92 Fontenay-aux-Roses (Seine), France
35. N. L. Bretz, Princeton Plasma Physics Laboratory, P.O. Box 451, Princeton, NJ 08544
36. J. D. Callen, Department of Nuclear Engineering, University of Wisconsin, Madison, WI 53706
37. R. W. Conn, Department of Chemical, Nuclear, and Thermal Engineering, University of California, Los Angeles, CA 90024
38. D. H. Crandall, ER-542 GTN, Office of Fusion Energy, U.S. Department of Energy, Washington, DC 20545
39. S. O. Dean, Fusion Energy Development, Science Applications, Inc., 2 Professional Drive, Gaithersburg, MD 20760
40. Documentation S.I.G.N., Department de la Physique du Plasma et de la Fusion Controlee, Centre d'Etudes Nucleaires, B.P. No. 85, Centre du Tri, 38041 Cedex, Grenoble, France
41. G. A. Eliseev, I. V. Kurchatov Institute of Atomic Energy, P.O. Box 3402, 123182 Moscow, U.S.S.R.
42. D. Evans, Culham Laboratory, Abingdon, Oxon. OX14 3DB, United Kingdom
43. M. Forrest, JET, Culham Laboratory, Abingdon, Oxon. OX14 3DB, United Kingdom

44. H. K. Forsen, Bechtel Group, Inc., Research Engineering, P.O. Box 3965, San Francisco, CA 94105
45. J. R. Gilleland, GA Technologies, Inc., Fusion and Advanced Technology, P.O. Box 85608, San Diego, CA 92138
46. V. A. Glukhikh, Scientific-Research Institute of Electro-Physical Apparatus, 188631 Leningrad, U.S.S.R.
47. R. W. Gould, Department of Applied Physics, California Institute of Technology, Pasadena, CA 91125
48. C. Gowers, JET, Culham Laboratory, Abingdon, Oxon. OX14 3DB, United Kingdom
49. R. A. Gross, Plasma Research Laboratory, Columbia University, New York, NY 10027
50. F. C. Jahoda, Los Alamos Scientific Laboratory, University of California, P.O. Box 1663, Los Alamos, NM 87545
51. Library, Culham Laboratory, UKAEA, Abingdon, Oxfordshire, OX14 3DB, England
52. Library, FOM Institut voor Plasma-Fysica, Rijnhuizen, Jutphaas, The Netherlands
53. Library, Institute of Physics, Academia Sinica, Beijing, People's Republic of China
54. Library, Institute of Plasma Physics, Nagoya University, Nagoya 464, Japan
55. Library, International Centre for Theoretical Physics, Trieste, Italy
56. Library, Laboratorio Gas Ionizzati, Frascati, Italy
57. Library, Plasma Physics Laboratory, Kyoto University, Gokasho Uji, Kyoto, Japan
58. N. C. Luhmann, 7702 Boelter Hall, Electrical Engineering Department, School of Engineering and Applied Science, 405 Hilgard Ave., University of California, Los Angeles, CA 90024
59. K. McCormick, Max-Planck Institut fuer Plasmaphysik, 8046 Garching bei Munchen, West Germany
60. D. M. Meade, Plasma Physics Laboratory, Princeton University, P.O. Box 451, Princeton, NJ 08544
61. R. R. Patty, Dept. of Physics, North Carolina State Univ., Raleigh, NC 27650
62. Plasma Research Laboratory, Australian National University, P.O. Box 4, Canberra, A.C.T. 2000, Australia
63. D. H. Priester, ER-542 GTN, Office of Fusion Energy, U.S. Department of Energy, Washington, DC 20545
64. P. J. Reardon, Brookhaven National Laboratory, Upton, NY 11973
65. D. D. Ryutov, Institute of Nuclear Physics, Siberian Branch of the Academy of Sciences of the U.S.S.R., Sovetskaya St. 5, 630090 Novosibirsk, U.S.S.R.
66. I. Spigel, Lebedev Physical Institute, Leninsky Prospect 53, 117924 Moscow, U.S.S.R.
67. W. M. Stacey, Jr., School of Nuclear Engineering, Georgia Institute of Technology, Atlanta, GA 30332
68. D. Steiner, Rensselaer Polytechnic Institute, Troy, NY 12181

69. J. D. Strachan, Princeton Plasma Physics Laboratory, P.O. Box 451, Princeton, NJ 08544
70. Thermonuclear Library, Japan Atomic Energy Research Institute, Tokai, Naka, Ibaraki, Japan
71. V. T. Tolok, Kharkov Physical-Technical Institute, Academical St. 1, 310108 Kharkov, U.S.S.R.
72. R. Varma, Physical Research Laboratory, Navrangpura, Ahmedabad, India
73. M. A. Walker, 199 Warren St. NE, Atlanta, GA 30317
74. M. Yamanaka, Dept. of Applied Physics, Osaka University, Yamada-kami, Suita, Osaka 565, Japan
75. K. M. Young, Princeton Plasma Physics Laboratory, P.O. Box 451, Princeton, NJ 08544
76. S. Zweben, Princeton Plasma Physics Laboratory, P.O. Box 451, Princeton, NJ 08544
- 77- Given distribution as shown in TIC-4500 under UC-20f
202. MFE-Experimental Plasma Physics

